ISSN: 2366-1313

# Modeling and Simulation of Micro electro mechanical Ultrasonic Transducer Based on Silicon Carbide

Suneeta Seelam, Research Scholar, Department of Electronics and communication Engineering, Monad University, Hapur, U.P.

Dr.Jaidev Sharma, Associate Professor, Supervisor, Department of Electronics and communication Engineering, Monad University, Hapur, U.P.

**Abstract:**

A collection of tiny devices that link mechanical and electrical components is known as a micro electromechanical system (MEMS). It is produced using batch processing methods that are compatible with integrated circuits (ICs) in sizes ranging from millimeters to micrometers. They have the ability to perceive their surroundings, control their responses, and act at a micro-scale. To produce impacts at a larger size, they may act alone or in groups. MEMS is a cutting-edge technology that dates back to the late 1970s. New possibilities for biological, chemical, and biological actuators and sensors have been made possible by technology. Although MEMS technology has its origins in IC production techniques, the test methodologies used by MEMS are crucial. MUTs come into two categories: piezoelectric and capacitive. Many piezoelectric ultrasonic micromachined transducers (PMUTs) have been created in the past and have been widely used for clinical imaging. For sensing or actuating, it often uses lead-zirconate-titanate (PZT) film. To address the flaws in piezoelectric transducers, capacitive ultrasonic micromachined transducers (CMUTs) were created in the field of research. These devices may be made using a high-temperature fusion bonding method or by employing a surface micromachining technique. The diaphragms of a typical CMUT are built using hexagonal, circular, or square geometry and are attached at the bottom by a fixed electrode. The top electrode operates as a diaphragm and the device acts as a variable capacitor since the functioning of this transducer is based on capacitive activities. Against the bottom electrode, it has the ability to move and alter form. This is why a change in the distance between these two electrodes causes a variance in capacitance. As a result, it is thought of as a capacitor cell made of a moving film that rests on the vacuum gap. The electrode that acts as the capacitor's electrode may be found on the device's top

ISSN: 2366-1313

and may be made of metal. Resonance develops in transmitting mode due to the biasing of the signal and the superimposed signal onto the geometry.

## 1 Introduction

Micro electro mechanical systems (MEMS), which are produced in sizes ranging from micrometers to millimeters using integrated circuit (IC) compatible batch-processing techniques, are a collection of microdevices that link mechanical parts and electrical components. These systems have the ability to detect, control, and react at the microscale. They may then act alone or in groups to produce effects at the macroscale. MEMS has evolved as a ground-breaking technology since the mids, creating new opportunities for chemical, physiological, and biological sensors and actuators. MEMS technology is based on IC manufacturing methods, however its test procedures vary greatly from those of ICs. Both electrical and data inputs from the environment are processed by MEMS devices. We are now able to create equipment that is so tiny that it is invisible to the human eye thanks to technological breakthroughs. MEMS devices are often measured in micrometers in terms of size. In a processing chip using new materials, it is now possible to mass manufacture thermal sensors, pressure gauges, accelerometers, viscoelastic actuators, repeaters, levers, gears, power transmitters, micro-mirrors, control valves, pumps, and motors on the same microdimensional level.

Mechanical microstructural components, microsensors, embedded systems, and microelectronic devices are all combined onto a single silicon chip in the most basic version of MEMS. A schematic representation of MEMS components is shown in Fig. 1.1. Microsensors accurately measure mechanical, thermal, magnetic, chemical, or electromagnetic information or events to detect changes in the environment of the system. Data is processed by microelectronics, which then sends signals to tiny actuators that respond and modify the surroundings. MEMS devices are very small and made up mostly of tiny pieces. As seen in Fig. 1.2, MEMS has been utilized to create everything from switches to gears to pistons to propellers and even steam turbines. MEMS encompasses more than simply the manufacture of silicon devices or the shrinking of mechanical parts. MEMS is a manufacturing process that uses batch fabrication techniques to create intricate mechanical systems and

ISSN: 2366-1313

gadgets as well as the electronics that go with them.

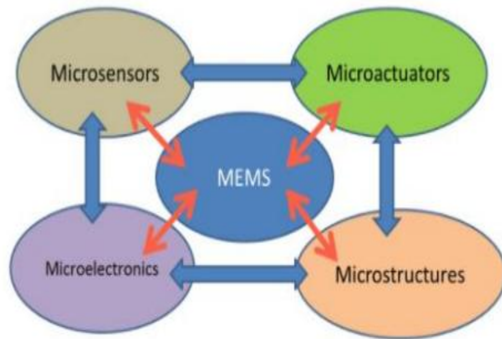


**Fig. 1.1** Components of MEMS

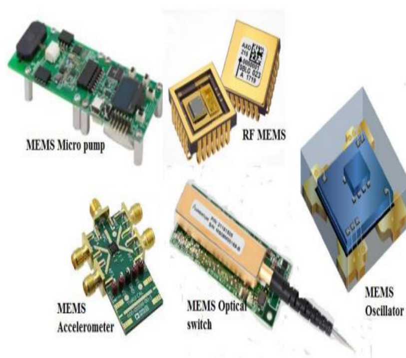


Fig. 1.2 Application of MEMS [6]

A large range of microsensors with useful sensing paradigms, such as heat, stress, surface tension, chemical reactions, electromagnetic field, radiation, and others, have been developed by MEMS practitioners and researchers during the last several decades. Surprisingly, several of these micromachined sensors have performed better than their macroscale counterparts. In addition to having excellent performance, MEMS devices are produced utilizing batch manufacturing techniques that are comparable to those used in the IC sector, which may lead to reduced production costs per device as well as a number of other advantages. As a consequence, superior device performance may be obtained and may even be offered at a fair price. Discrete silicon microsensors were quickly brought to market, and their applications are now expanding quickly. Recently, the MEMS research and development community has demonstrated micropumps to create positive fluid pressures, microflaps, independently controlled micromirror arrays for displays, optoelectronic devices and reflectors to redirect or control light beams, and microvalves for controlling gas and liquid flows. These tiny actuators can execute mechanical feats far bigger than their size would imply, which means that despite their small size, they may often cause macroscale effects. Scientists have proved that these microminiaturized devices are capable of guiding the aircraft on their own by attaching tiny micro actuators to the leading edge of an airplane's air foils.

An acoustic sensor known as an ultrasound transducer turns alternating voltages into ultrasound or, conversely, turns ultrasound into an electrical signal. As shown in Fig. 1.3, ultrasounds often utilized in applications including medical imaging, non-destructive testing (NDT) [7-8], sonar, flow metering [9-10], and ultrasonic range measurement

ISSN: 2366-1313

occur at frequencies beyond hundreds of kilohertz, which are greater than the threshold of human hearing.

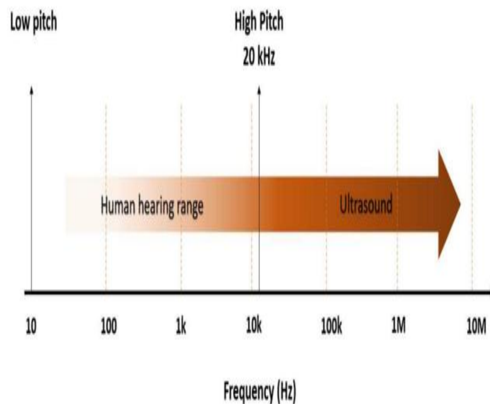


Fig. 1.3 Frequency range of ultrasound wave

**2 Litreature Survey**

Sensing and actuation are only two of the many uses for ultrasound. In all of these industrial cleaning applications, therapeutic techniques including lithotripsy, tissue ablation, and ultrasound detection are essential. The coupling medium from the source must be used to detect the imparted ultrasonic. Wafer temperature is measured using a solid coupling medium; liquid is utilized for NDE and medical applications; and gas is used for air-coupled applications. When utilized in fluid-coupled applications, a piezoelectric transducer has an impedance mismatch. MUTs are often used in acoustic and high-dynamic-range air transducer applications.

Both ultrasonic microscopy and ultrasound flow metering in medical treatment have been extensively researched. Since theoretical study inhibits actual implementation, there are still a lot of unexplored application areas. The necessity for piezoelectric transducers has decreased as a result of the capacitive transducer's success in acoustic applications, impedance matching, wide bandwidth, and high-frequency applications. It is much less costly than a piezoelectric transducer since photolithography is used. An insulating layer sits on top of a conductive Si substrate to form the bottom electrode of a micro-dimensional capacitive element. An actuation layer made of metalized polysilicon that is conducting is printed onto the top electrode. An insulation layer on the conductive substrate prevents parallel electrodes from touching one another and, by insulating the device, raises the collapse voltage. Acoustic sensors have been utilized for underwater imaging since the early 20th century. At the turn of the century, a critical mass had been achieved in the development of piezoelectric materials. Significant advancements in computer technology call for increasingly complex algorithms for transducer performance assessment. Through the use of micro fabrication

ISSN: 2366-1313

technology, air gaps are decreased as a consequence of technical empowerment. In order to compete with piezoelectric sensors, capacitive electrostatic transducers may generate strong electric fields. Enhanced uses of CMUTs include integration with microelectronics, higher bandwidth, and huge arrays with connected electrical connections.

Rapid advancements in characterisation methods and a sound understanding of functioning principles have both significantly enhanced. The device's conception, manufacture, and methods are all improved by a fruitful behavioral approach research. Non-contact optical profilometers, which use optical interferometry to scan the surface of the CMUT in a microscopic environment, are significantly impacted by the CMUT's static behavior. The formulas demonstrate a relationship between the input and output variables as well as the structural requirements using finite element method (FEM) simulation. The benefits of CMUTs are many, and they include increased bandwidth, massive manufacturing techniques, superior sensitivity, and short reaction times.

Due to intensive research, CMUTs have lately been able to overcome the difficulties of fabricating two-dimensional arrays and are now able to capture real-time three-dimensional pictures. High power transmission requires a collapsed mode CMUT with correct biasing [18–19]. It is difficult to make an air-coupled ultrasonic transducer array that runs at 40 KHz and doesn't have grating lobes. When doing acoustic imaging in the presence of air, the size of the grating lobes presents a restriction. A one-dimensional air-coupled phased array transducer that can operate at 40 KHz is created by excluding the grating lobes. This obstacle may be avoided by keeping the transducer size under 4.3 mm.

Many researchers have created various manufacturing methods for CMUT. These techniques include wafer bonding, bulk micromachining, and surface micromachining. They may also be combined. At Stanford University, surface micromachining was used to manufacture CMUT for the first time. This procedure involves the formation of a bottom electrode on a non-conductive substrate, followed by the deposition of a sacrificial layer. By pre-patterning the sacrificial layer and afterwards constructing an anchor with the membrane around it, as illustrated, better dimensional control of the membrane is accomplished in this procedure. The membrane's structural layer is then placed on top of it, and release apertures

ISSN: 2366-1313

are used to etch it. By removing the sacrificial layer, the membrane of the device is therefore hung onto the substrate.

Metallization is often carried over to the membrane in order to make it conduct. If the gadget is exposed to liquid, protection is achieved by placing a final sealing layer. Electronics and surface-micromachined CMUT have both been tried to combine by several researchers. An IC substrate was electrically connected to the CMUT array via a flip-chip bonding through silicon. As the CMUT membrane and the IC metallization layer serve as a sacrificial layer to construct the cavity after metal has been etched, IC dielectric layers are involved. The oxide layer serves as a sacrificial layer while the polysilicon layer serves as a membrane material. Additionally, an alternate method of fabricating transducers may be used after the IC is finished. Here, PECVD silicon nitride membrane is successfully used to fabricate CMUT on top of an IC substrate while sputtering chromium into a protective layer at 250°C.

To produce a capacitive gap using wafer bonding methods, cavities are etched directly onto a wafer rather than contacting the sacrificial layer. The membrane layer is suspended atop a handle wafer during the bonding of this wafer with another substrate. The thin CMUT membranes are maintained suspended in etched cavities until the handle wafer is eventually dissolved from the double-bonded substrates. There are two benefits to the wafer bonding technique. First, a superior epitaxial film with strict thickness control is used to create the membrane layer. As a result, reliability and thickness uniformity are improved for large-sized membranes.

## 3 Methododlogy

The electrostatic transduction mechanism based on capacitive action is the fundamental working concept of the CMUT. This capacitive action is created between a stationary electrode and a moving, vibrating electrode. The gadget must have a bias in order to operate properly in active mode. Additionally, a signal must be applied between the top moveable electrode and the bottom fixed electrode while being overlaid on the bias voltage. As a result, the electrostatic force that results is altered, which creates vibration in the actuation layer as seen in Fig. 1. Ultrasound is then produced at the same frequency and overlaid over the bias. The actuation layer is drawn toward the substrate by the force of electrostatic attraction as a result of the application of bias between

ISSN: 2366-1313

two electrodes. This attraction force was created using the columbic force theory.

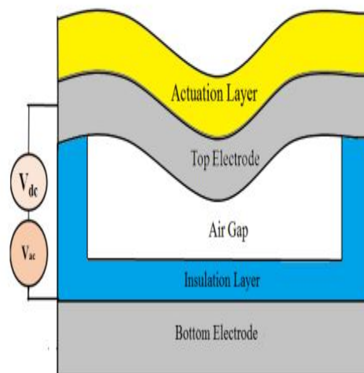


Fig. 4.1 2D model of biased actuation layer vibration in circular CMUT

Bias application provides the charge that the vibrating structural layer modulates, and ultrasound is produced for electrostatic actuation. Bias is crucial for achieving harmonic movement of the actuation layer in the transmission mode. The consequent bending firmness and residual stress of the structural material serve to balance the electrostatic force that is generated.

Capacitive transducers are mostly used as electrostatic transducers since they can function in strong electric fields. More than 108V/cm of an electric field may be generated by it. To preserve repeatability and precision during the working condition with a strong electric field, proper handling must be observed [3]. In compared to piezoelectric and magnetostrictive transducers, the device is preferable due to its excellent mechanical impedance matching with the environment. Numerous research publications examine hexagonal, square, and circular components according to the form of the structural layer. One of these structures, the hexagonal transducer, operates across a wide temperature range and requires very little money to make. Circular shapes are extensively used in applications that need lengthy distances under water and strong system repeatability. Additionally, this structure has exceptional sensitivity when used for medical imaging.

Numerous research publications have offered additional device characteristics and analytical models since this study takes a circularly shaped cell into account. These investigations used approximations while taking into account the capacitive action of parallel plates. Later, by taking into account the pull in voltage and characteristics generated from the equivalent circuit model, the computation of the real deflection of the moveable edge clamped top electrode was developed. The top electrode was treated as a plate in this study and the impact of a non-uniform load was taken into account while resolving the structure. In the study, the Galerkin approach was taken into account for resolving the electrostatic action on a plate that was loaded concentrically. A change in

electrostatic force will occur owing to variation in their separation as a result of increasing bias voltage, which generates an uneven load distribution onto the top electrode. It is no longer required to treat the top electrode as a plate if its deflection does not exceed 50% of the gap separation during pull-in conditions. thus in For the deflection of a circular plate, a straightforward solution is taken into consideration.

**4 Results & evaluation**

Contrarily, implementing the idea of series expansion via the solution of a square diaphragm using trigonometric or polynomial basis functions is stated in paper. In a second combined method, the research studies the electrostatic action that results in deflection while taking into account both the circular and square geometrical form functions. a mass-spring-damper electromechanical model that was used in a study to represent the behavior. In several research papers, the electrostatic force is calculated using the fringe idea. The device's capacitance is increased by the fringing field's impact; as a result, electrostatic force was also impacted. It could be feasible to build their connection using the Younes Ataiiyan's approach in a circular-disk capacitor. As a result, this additional force improves the structural layer's displacement profile.

The fringing effect is caused by the presence of bending electric field lines at the capacitive plate and is further explained in Chapter 3. Increased device equivalent capacitance as a result of fringing has an impact on the electrostatic force produced in the CMUT. According to Fig. 3.2(b), an analytical calculation of force is performed in a non-insulated cell with a completely metalized actuation layer while taking into account capacitance modeling and the CMUT structure [20]. Potential energy determines what 'u' is. The formula used to compute u is

$$u = \frac{1}{2} C_{eq} v(t)^2$$

where, Ceq represents the direct series capacitance of actuation layer capacitance, Ca and the air gap capacitance, Cg resulting in an effective electrostatic force as in (4.2),

$$F = -\frac{du}{dt_g}$$

Putting the value of ( 4.1) in ( 4.2) , force can be expressed as

$$F = -\frac{du}{dt_g} = -\frac{1}{2} v(t)^2 \frac{dC_{eq}}{dt_g}$$

Here v(t) is applied voltage between two electrodes and tg is air gap. Putting the

device equivalent capacitance from (3.4), the following expression becomes,

$$\frac{dC_{eq}}{dt_g}=\frac{d}{dt_g}\left(\frac{C_a\times C_g}{C_a+C_g}\right)=C_a\frac{d}{dt_g}\left(\frac{C_g}{C_a+C_g}\right) \quad (4.4)$$

$$=\frac{C_a\left[(C_g+C_a)\frac{dC_g}{dt_g}-C_g\frac{d}{dt_g}(C_g+C_a)\right]}{(C_g+C_a)^2}$$

$$=\frac{C_a^2}{(C_g+C_a)^2}\cdot\frac{dC_g}{dt_g} \quad (4.5)$$

As, $\frac{dC_g}{dt_g}=\varepsilon_g\left[\frac{-\pi r_e^2}{t_g^2}\right]$, hence putting the value of $\left(\frac{dC_g}{dt_g}\right)$ and (4.5) , (4.3) can be rewritten as,

$$F=-\frac{du}{dt_g}=-\frac{1}{2}\frac{v(t)^2C_a^2}{\left(\frac{C_a}{C_g}+1\right)^2C_g^2}\times\frac{dC_g}{dt_g}$$

$$F=\frac{1}{2}\frac{v(t)^2C_a^2}{C_g^2\left(\frac{C_a}{C_g}+1\right)^2}\left[\varepsilon_g\frac{\pi r_e^2}{t_g^2}\right] \quad (4.6)$$

The force on the actuation layer including the fringing capacitance, (4.3) can be rewritten as,

$$F_f=-\frac{1}{2}v(t)^2\frac{dC_{eqf}}{dt_g}$$

Hence, putting the device equivalent capacitance from (3.9), the following expression becomes,

$$\frac{dC_{eqf}}{dt_g}=\frac{d}{dt_g}\left(\frac{C_{af}\times C_{gf}}{C_{af}+C_{gf}}\right)=C_{af}\frac{d}{dt_g}\left(\frac{C_{gf}}{C_{af}+C_{gf}}\right) \quad (4.8)$$

$$\frac{dC_{eqf}}{dt_g}=\frac{C_{af}\left[(C_{gf}+C_{af})\frac{dC_{gf}}{dt_g}-C_{gf}\frac{d}{dt_g}(C_{gf}+C_{af})\right]}{(C_{gf}+C_{af})^2}$$

$$=\frac{C_{af}\left[(C_{gf}+C_{af})\frac{dC_{gf}}{dt_g}-C_{gf}\frac{d}{dt_g}(C_{gf}+C_{af})\right]}{(C_{gf}+C_{af})^2}$$

Putting the value of (3.7) & (3.8), $\frac{dC_{gf}}{dt_g}$ can be written as (4.10)

$$\frac{dC_{gf}}{dt_g}=-\varepsilon_g\left[\frac{\pi r_e^2}{t_g^2}+\frac{r_e}{\frac{16\pi r_e}{t_g}-1}\cdot\frac{16\pi r_e}{t_g^2}\right]$$

Putting (4.10) in (4.9), the expression can be rewritten as,

$$\frac{dC_{eqf}}{dt_g}=\frac{-C_{af}^2\varepsilon_g}{(C_{gf}+C_{af})^2}\left[\frac{\pi r_e^2}{t_g^2}+\frac{r_e}{\frac{16\pi r_e}{t_g}-1}\cdot\frac{16\pi r_e}{t_g^2}\right]$$

Hence considering (4.11) and putting the value in (4.7) electrostatic force is expressed as (4.12)

$$F_f=\frac{1}{2}\frac{v(t)^2C_{af}^2}{C_{gf}^2\left(\frac{C_{af}}{C_{gf}}+1\right)^2}\left[\varepsilon_g\frac{\pi r_e^2}{t_g^2}+\frac{\varepsilon_g r_e}{\left(\frac{16\pi r_e}{t_g}-1\right)}\times\frac{16\pi r_e}{t_g^2}\right] \quad (4.12)$$

A comparative analysis is accomplished altering the actuation layer by SiC instead of Si3N4. To generate appreciable amount of electrostatic force in resonance with the operating frequency a large bias is delivered along than the signal.

Expression of total voltage is, $v(t)=V_{dc}+V_{ac}cos\omega t$, where $V_{dc}$ is the bias and $V_{ac}$ is the signal. Hence, $v(t)^2=V_{dc}^2+2(V_{dc}V_{ac})\cos\omega t+V_{ac}^2\cos^2\omega t$

V t is the second harmonic, which is quite less compared to the bias . As the applied bias is considerably greater than time varying one, considering the electrostatic force for applied bias (4.6) and (4.12) can be rewritten as,

ISSN: 2366-1313

$$F_{bias} = \frac{1}{2}\frac{V_{dc}^2 C_a^2}{C_g^2\left(\frac{C_a}{C_g}+1\right)^2}\left[\varepsilon_g \frac{\pi r_e^2}{t_g^2}\right]$$

$$F_{f_{bias}} = \frac{1}{2}\frac{V_{dc}^2 C_{af}^2}{C_{gf}^2\left(\frac{C_{af}}{C_{gf}}+1\right)^2}\left[\varepsilon_g \frac{\pi r_e^2}{t_g^2} + \frac{\varepsilon_g r_e}{\left(\frac{16\pi r_e}{t_g}-1\right)} \times \frac{16\pi r_e}{t_g^2}\right]$$

Dynamic electrostatic force for signal is expressed as,

$$F_{f_{signal}} = \frac{V_{ac} V_{dc} C_{af}^2}{C_{gf}^2\left(\frac{C_{af}}{C_{gf}}+1\right)^2}\left[\varepsilon_g \frac{\pi r_e^2}{t_g^2} + \frac{\varepsilon_g r_e}{\left(\frac{16\pi r_e}{t_g}-1\right)} \times \frac{16\pi r_e}{t_g^2}\right]$$

The device that uses SiC as an actuation layer creates electrostatic force bias SiC () Ff, while the identical device that uses Si3N4 also generates electrostatic force as () 3 4 bias Si N Ff. The relative dielectric constants are 9.7 and 7.5, respectively, in (4.7), and these values of electrostatic force are obtained from Ceqf SiC () and 3 4 Ceqf Si N () using (3.8).

Fig. 4.2 depicts the equivalent electric potential profile with the fringing field line. PZFlex is a system of user-defined units. We've added symmetry to the model to make it easier to understand. The structure is separated into two equal halves using symmetry criteria to make analysis easier and reduce simulation run time. In the parametric sweep of the investigation, a dc bias of 40V is applied for the parametric analysis of electrostatic potential. When choosing an electrostatic study, an electrostatic potential is supplied to the top surface of the bottom electrode and the border between the actuation layer and bottom electrode. After that, a mesh is created and calculations are run.

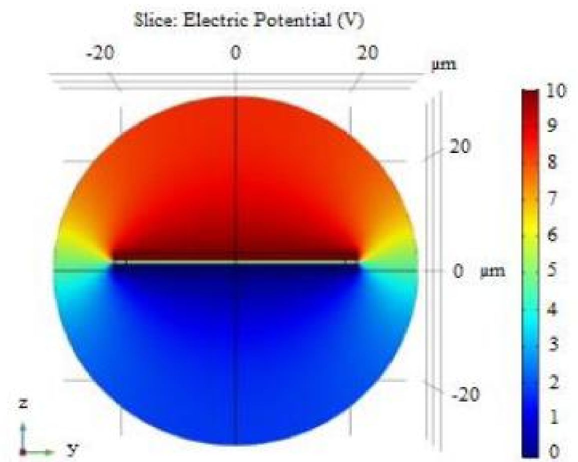


Fig. 4.2 Electric potential profile

This section discusses how electrostatic force behaves in relation to several factors, including electrode radius, air gap, actuation layer thickness, and bias of actuation layer-based CMUT. The electrostatic force's behavior in response to an electrode radius change is seen in Fig. 4.3. Increased device capacitance is caused by an increase in electrode radius, which also increases electrostatic force. Fringing causes an increase in

ISSN: 2366-1313

electrostatic force that is represented as

$$E_F = \left( \frac{F_{f_{bias}} - F_{bias}}{F_{bias}} \right) \times 100 \quad (4.16)$$

Enhancement in a cell with SiC actuation layer instead of $Si_3N_4$ is

$$E_{F_SiC} = \left( \frac{F_{f_{bias(SiC)}} - F_{f_{bias(Si_3N_4)}}}{F_{f_{bias(Si_3N_4)}}} \right) \times 100 \quad (4.17)$$

According to Fig. 4.4, the average EF for Si3N4 and SiC actuation layers respectively is 13% and 15%. For smaller radius values, fringe effects are more pronounced. Additionally, Fig. 4.5 shows a plot of the electrostatic force augmentation in the SiC cell as compared to the Si3N4 cell.

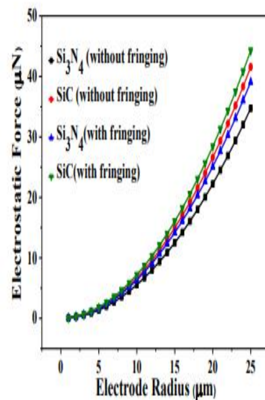


Fig. 4.3 Electrostatic force due to variation in electrode radius

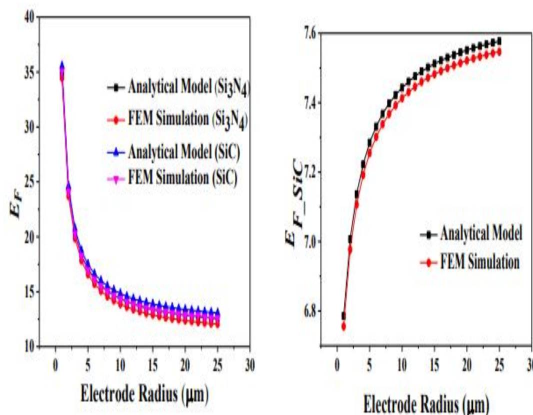


Fig. 4.9 depicts the electrostatic force's variation in relation to the actuation layer's thickness. After 300 nm, an increase in actuation layer thickness adds more to force augmentation. In Figs. 4.10 and 4.11, a plot of EF and EF SiC _ is shown in relation to actuation layer thickness. A drop in capacitance occurs when the actuation layer's thickness increases the distance between its two electrodes, which in turn lowers the electrostatic force. The increasing thickness of the actuation layer, which results in an average EF of 11.89% for Si3N4 and 13.13% for SiC, undoubtedly has a significant influence on the contribution of fringing. An average EF SiC _ of 17.7% occurs as a result of fringing.

**5 Conclusion**

The acoustic pressure from a CMUT may be calculated analytically using piston vibration analysis under the assumption that the CMUT membrane is a piston positioned on a rigid planar boundary. The piston model was used under a number of presumptions, excluding the influence of hard edges as well as the interaction with all currently recognized physical domains. A DC voltage range of 0 to 80 V was used. When the hexagon's side or radius is expanded, the collapse voltage falls. the pull-in or collapse-voltage plot along the

ISSN: 2366-1313

hexagon's side and radius for circular and hexagonal CMUT. The pull-in voltage differential inaccuracy between circular and hexagonal CMUTs is 20.9%. The disparity might be explained by the fact that whereas in a circle, every point on the periphery is equally distance from the center, this is not the case in a hexagon. Not all of the spots are equally far from the center.

When the CMUT membrane is compared to the piston model with the assumption of a lesser deflection as compared to the lateral dimension of the membrane, the characteristics of the axial acoustic pressure at positions close to and far from the source are shown. The characteristics of CMUT are revealed. The created acoustic pressure wave exhibits amplitude variations in the vicinity of the source, or the "near field."

**6 Reference:**

[1] Seyed M Allameh 2006 Advanced Structural Materials: Properties, Design Optimization, and Applications.

[2] P Muralt 2000 Ferroelectric thin films for micro-sensors and actuators J. Micromech. Microeng. 136–146.

[3] N Setter, D Damjanovic, L Eng, G Fox, S Gevorgian, S Hong et.al 2006 Ferroelectric thin films: Review of materials, properties and applications Journal of Applied Physics 100.

[4] Wasa K, Kanno I, Kotera H, Yamauchi N, Matsushima T 2008 Thin films of PZT-based ternary perovskite compounds for MEMS Proc. of IEEE International Ultrasonics Symp, 213-216.

[5] Zhang Z, Li X and Chen 2000 J, Journal of Tianjin University 33 378-381.

[6] Naoki W, Kazumasa K and Yi X 2000 Thin Solid Films 372 156-162.

[7] L HENCH and J WEST 1990 The Sol-Gel Process, Chem.Rev. 90 33-72.

[8] I Y (Steve) Shen, G Z Cao, Chia-Che Wuand Cheng-Chun Lee 2006 PZT Thin-Film Meso- and Micro Devices Ferroelectrics 342 15–34.

[9] Klein L 1994 Sol-Gel Optics: Processing and Applications Springer Verlag. ISBN 0792394240.

[10] Hirano S I, Yogo T and Tikuta K 1992 J Am. Ceram. Soc.75 2785-90.

[11] S K Pandeya, A R Jamesa, R Ramana, S N Chatterjeea et.al 2005 Structural, ferroelectric and optical properties of PZT thin films Physica B, science direct 369 135–142.